



Modelling of the trade-off between the deep soil moisture and vegetation restoration in the hilly area of the Loess Plateau, China

Yuqing Chang^a, Lei Han^{a,b,*}, Rui Chen^a, Zhao Liu^a, Yabei Li^a, Zilin Zhao^a, Yifeng Gao^a, Meili Yang^a, Xinxin Cao^a, Zheyuan Miao^a, Hongliang Kang^a

^a School of Land Engineering, Shaanxi Key Laboratory of Land Consolidation, Chang'an University, Xi'an, China

^b State Key Laboratory of Loess and Quaternary Geology, Institute of Earth Environment, CAS, Xi'an, China



ARTICLE INFO

Handling Editor: Y. Huang

Keywords:

Soil moisture
Landscape pattern
Trade-off analysis
Hilly area of the loess plateau

ABSTRACT

Excessive depletion of soil moisture by artificial forests in the vegetation restoration areas of the Loess Plateau has attracted widespread attention. To assess potential risks of soil moisture deficit, we needed on-site vegetation and soil sampling data, as well as UAV images from the Chaigou Watershed for three-dimensional analysis, combining both sampling and raster data. Three-dimensional surfaces for assessment of trade-off were established innovatively by the local regression and interpolation methods. The results indicated that soil moisture benefits at 20–40 cm depth are lower than at 0–20 cm due to infiltration and surface disturbance. In some areas of the Chaigou Watershed, grass and shrub-grass vegetation are facing risks of soil moisture deficit based on trade-off values (RSMD) and multiparameter evaluations. Analysis of deep soil water content variability revealed the moisture decreases significantly with the deepening of the soil layer in some plots. R (Richness), H (Shannon's Diversity), Margalef, COHESION, and CONTAG were applicable in interpolation and fitted with the local regression model ($R^2 > 0.6$) corresponding to the trade-off, but SPLIT was proven to be inapplicable in this study area. The zero trade-off inflection points were 6%–8%, while the trend inflection points were 7.5%–9% for soil moisture and vegetation indices of vegetation and landscape in typical sampling sites of the Chaigou Watershed. Three-dimensional fitting model is more comprehensive and effective in assessing deep soil moisture conditions and grass plots on shady slopes generally had the best trade-off status in this region.

1. Introduction

A prominent topic of debate in northern China in recent years has been the possible conflict between revegetation and protecting water resources (Ghimire et al., 2014; Lan et al., 2021). In an ecologically vulnerable dry and semiarid environment, soil moisture (SM) is essential for ecological stability and ecologically sustainable development (Fang et al., 2012). In the past 30 years, the amount of green vegetation coverage on the Loess Plateau of China (CLP) has increased significantly, soil and water conservation work has been effectively carried out, and the ecological environment has been significantly improved. However, plant transpiration was also increased by rapid vegetation planting, resulting in a deficit of soil moisture (Ghimire et al., 2014; Lan et al., 2021). It is no doubt that effective quantitative assessment methods are helpful in assessing the ecological environment status of arid areas.

A trade-off analysis can be applied to detecting relationships and variable trends across multiple elements to reveal complex interaction

mechanisms (Bradford and D'Amato, 2012). The root mean square deviation (RMSD) was effectively proven to assess the soil moisture status in vegetation restoration areas with plant diversity indices (Liu et al., 2019; Su et al., 2021; Wang et al., 2017; Wang et al., 2020; Fischer et al., 2019). For example, several researchers were selected multiple plant diversity indices as vegetation characteristics to explore the relative benefits of soil water (Wang et al., 2020; Zhang et al., 2018), but lacking of studies about the trade-off between soil moisture and revegetation in arid zones due to several vegetation parameters. In pertinent research, the terms "shortage", "appropriateness", and "excess" were employed to describe the state of soil moisture (Han et al., 2022). Besides, deep soil moisture has a higher ecological value, but a lack of research on the trade-off of deep soil moisture in multiple layers (Jia and Shao, 2014; Tong et al., 2020). Most recent studies on soil moisture in the revegetation area involved shallow soil moisture because of the difficulties of sampling.

In order to better obtain valuable information from the measured

* Corresponding author at: State Key Laboratory of Loess and Quaternary Geology, Institute of Earth Environment, CAS, Xi'an, China.

E-mail address: hanshuanglei@chd.edu.cn (L. Han).

data, analyzing the data is a fundamental part of researches. In general, the distribution characteristics of the field survey data do not follow a normal distribution, and the data distribution has poor continuity, and the grouping discrete characteristics are obvious, which make it impossible for simple linear regression to accurately fit a process of trade-offs. Piecewise regression and nonparametric conditional quantile regression (NCQR) which widely used in medical and economic fields (Yun et al., 2014) has been proven suitable for revegetation and soil water (Han et al., 2022). With deeper soil layers, previously applicable 2D models must be modified to enhance dimensionality, and spatial fitting in 2D must be improved to 3D, while relevant research is currently lacking. It is worthwhile to investigate whether spatial interpolation in three-dimensional simulation could be employed in this study and provide a better method with landscape parameters in deep soil layers.

The Loess Plateau is an example of an environmentally vulnerable zone appropriate for vegetation restoration. Although research on vegetation restoration has made a lot of progress, excessive water

consumption from large-area revegetation. The dried soil layer and small old trees have also attracted attention (Li et al., 2021; Ma et al., 2022; Nan et al., 2019; Shi et al., 2020). In addition, the topographic relief in the steep slope has a great impact on SM (Wang et al., 2015), increasing the spatial variability of soil water due to surface radiation, with higher soil moisture on the shady slopes and downslopes (Gao et al., 2016; Melliger and Niemann, 2010).

To provide scientific reference for the adjustment of revegetation in semi-arid ecologically fragile areas, the trade-off between deep soil moisture and vegetation in the sampling sites was explored. In this study, the Chaigou Watershed were selected as the study area due to the typical climate and vegetation restoration. Besides, plant diversity indices, richness, vegetation cover, and evenness (Pielou index) obtained from field sampling plots were integrated, and models of local regression and non-parametric fitting and spatial interpolation were used to perform the fitting of multiple parameters from two-dimension to three-dimension for deep soil moisture.

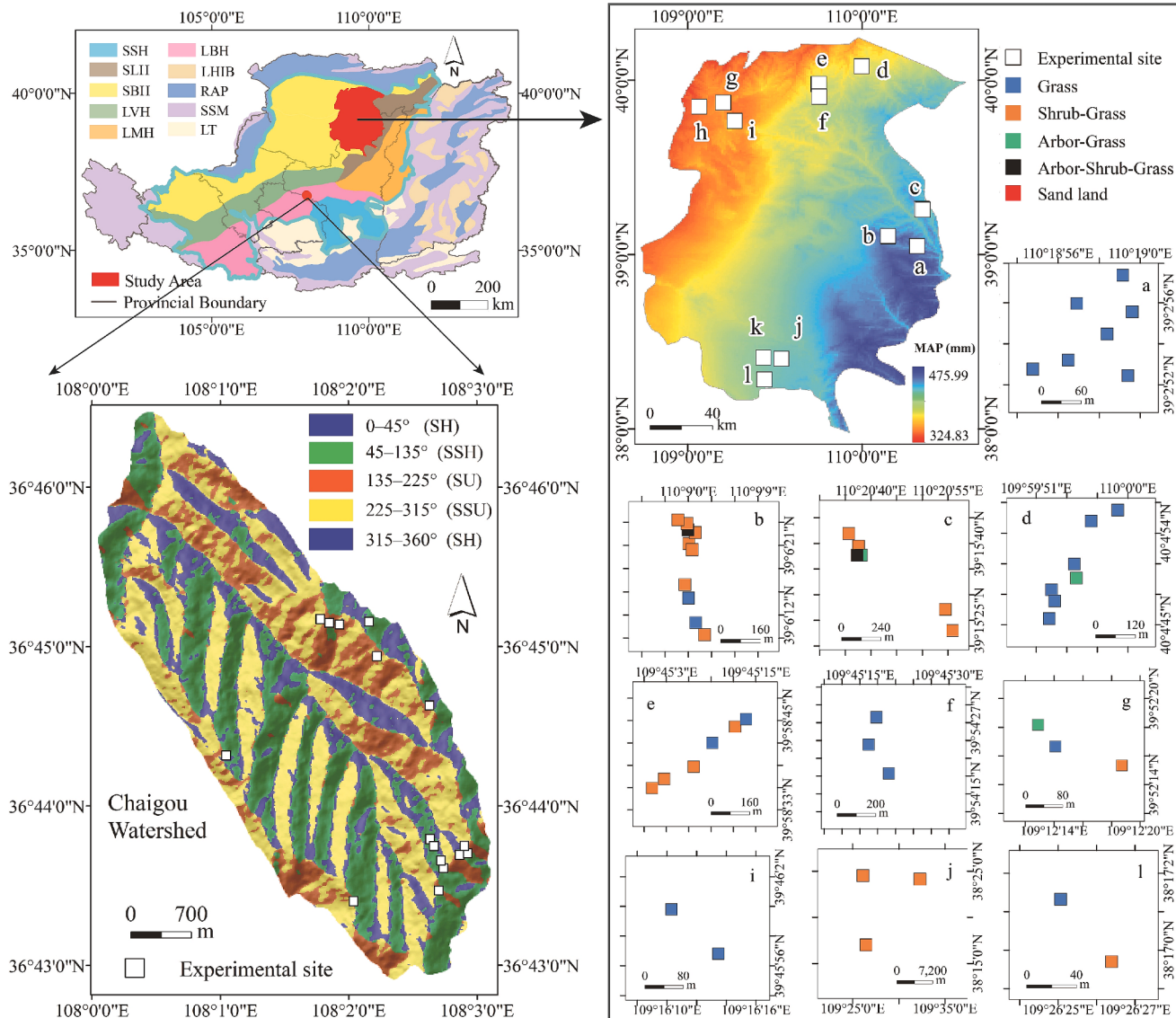


Fig. 1. The plots in CLP evaluating vegetation and soil water in medium and small-scale regions. Note: First sampling subregion ($n = 23$, a–c); second sampling subregion ($n = 16$, d–f); third sample subregion ($n = 6$, g–i); the last sampling subregion ($n = 5$, j–l). Different signs indicated different vegetation types. For Chaigou Watershed, Shady-slope (SH), Semi-Shady-slope (SSH), Sunny-slope (SU), and Semi-Sunny-slope (SSU) (Li et al., 2022). SSH, SLH, SBH, LVH, LMH, LBH, LHIB, RAP, SSM and LT were defined as soil stone hill, sandy loess hill, sandy loess hill, sand blown hill, loess valley hill, loess mound hill, loess beam hill, loess hills of intermountain basin, river alluvial plain, soil stone mountain and loess tableland, respectively.

2. Materials and methods

2.1. Study area and experimental design

The Loess Plateau is predominantly characterized by its hilly terrain, which encompasses around 56.79 percent of the total area. These hills span over the semi-humid and semi-arid region from east to west, exhibiting a distinct continental monsoon climate. The region experiences an average annual temperature ranging from 3.6–14.3 °C (Yang et al., 2019; Zhang et al., 2008), characterized by significant variations in both annual and daily temperatures. The climate is characterized by rainy summers and autumns, followed by dry winters and springs with minimal rainfall. Additionally, severe droughts occur during the spring season. Extensive vegetation surveys and soil sample collection were conducted as part of the research in the northern of hilly-gully in CLP in the previous study (Han et al., 2022). This study focuses on the Chaigou Watershed, which is a representative watershed for vegetation restoration. The objective of this research is to investigate the suitability of employing multi-parameter and multi-model fitting methodologies to analyze the trade-off scenario of soil moisture. To achieve this, the depth of sample collection was carefully determined.

Chaigou Watershed is located in northern Shaanxi (Wuqi, Yan'an, 108°0'2.19"E–108°3'6.859"E, 36°42'54.05"N–36°46'28.779"N) (Liang et al., 2006), part of the hilly and gully area in the CLP, located at the junction of Shaanxi, Gansu and Ningxia provinces (SGN) of China (Fig. 1). The research area of the Chaigou Watershed is about 15.15 km². The geomorphological type of this watershed is loess hilly and gully. The elevation ranges from 1489.36 m to 1794.76 m. In the research area, microtopography is found throughout the region and includes platforms, collapses, scarps, gullies, and shallow gullies. The area has a semiarid, moderate, continental monsoon climate similar to Wuqi County. It receives 483.4 mm of precipitation on average from June to September every year. According to some researches, the monthly temperature varies from –7.7 °C in January to 21.6 °C in July, with a mean value of 7.8 °C (Zhang et al., 2021). The majority of the vegetation at the moment in the natural restoration region of Chaigou Watershed is herbaceous. In specific, the designed restoration region of the Chaigou Watershed has a large amount of arbor, shrub, and herb.

The Chaigou Watershed, with typical topographic features of loess ridge and loess hills, is located in a loess hilly-gully region (Li et al., 2007). After our fieldwork in the summer of 2021, the vegetation growth was distinct for various slopes, and the dominant plant species were different on different slope locations in the same slope direction. Solar radiation is significantly weaker on north-facing slopes than on south-facing sunny slopes in the Northern Hemisphere, and the soil water content of shady slopes is relatively more, better plant growth and rich species diversity in the shady slopes. The planting of *Artemisia* on the upper slope of the sunny slope has a significant soil and water conservation effect, and it can weaken the runoff on the middle and lower positions. In general, the vegetation is more abundant at the bottom of the slope such as taller *Imperata cylindrica* and thicker branches of arbors.

2.2. The test sites

Upon an investigation of the spatial arrangement of the microtopography in the Chaigou Watershed, we selected the typical sampling plots of microtopography on four types of slope aspects (sunny, semi-sunny, shady, and semi-shady) because of variation in surface radiation. Thus, a total of 16 sampling plots were set up in our study sites, including cropland, forest, grass, orchard, construction land, economic forest trees, unused land, and water. Within the standard vegetation area, the sample plot sizes varied, the lengths of the square plots were 4 m, 6 m, and 10 m for grass, shrub/shrub-grass and arbor-grass/arbor-shrub-grass, respectively.

Grass, shrub-grass, arbor-grass, arbor-shrub-grass, apple orchard,

and cropland (mainly maize) were the primary six types of vegetation in the Chaigou Watershed, and the structures were visualized based on some realistic plant elements in Blender 3.2 (3D Graphic Imaging Software) (Fig. 2). In the hilly area, sampling plots were chosen based on topography, where the geo-information such as aspect and slope were extracted by DEM (Digital Elevation Model). Sixteen typical plots in the Chaigou Watershed were selected for further exploration that six types of vegetation and corresponding slope aspect. However, the vegetation combination type of arbor-shrub-grass was only found on sunny and semi-sunny slopes in hilly areas. It was derived from the process of vegetation restoration and vegetation succession, where tall forests block the sunlight needed for the growth of shrubs. It was difficult for the type of vegetation containing shrubs to grow healthily where sunlight radiation was not sufficient.

Additionally, the surface soil (at 0–5 cm) was removed, and each sampling plot was divided into 11 layers vertically downwards from the surface, i.e., 5–10 cm, 10–20 cm, 20–40 cm, 40–60 cm, 60–80 cm, 80–100 cm, 100–120 cm, 120–140 cm, 140–160 cm, 160–180 cm, 180–200 cm. The depths of soil layers for the collection were set at variable intervals including 5 cm, 10 cm, and 20 cm due to the susceptibility of the upper soil layer to disturbance. For precise weighing and storage easily, a 10,000-point balance (FA2004B) was used. As the weight of the soil sampling plastic tube plus soil was more than 200 g, to not exceed the range, soil samples must be divided for the weight of the wet soil sample immediately, 0–20 cm just with one self-sealing bag, but 20–200 cm with two small self-sealing bags. A total of 320 bags of soil samples were obtained from field sample collection. After a period of air-dried by opening the bags at room temperature, they were then dried in an electric heating blast drying oven to dry at 105 °C to a constant weight (Li et al., 2016). The mass of the container in which the soil sample was stored as well as the self-sealing bag had been subtracted from the calculation. The formulas for calculating the soil water content (g/g) by the drying method were simplified as follows (Chen Lifang et al., 2019):

$$SM_i = \frac{M_{wet,i} - M_{dry,i}}{M_{dry,i}} \quad (1)$$

where SM_i is the soil moisture in plot i ; $M_{wet,i}$ and $M_{dry,i}$ are the mass of soil (plot i) in wet and dry conditions.

2.3. Calculation of vegetation parameters and trade-off

The relevant vegetation parameters, richness, Shannon-Wiener, Margalef, Simpson and evenness, were selected and calculated in terms of the vegetation growth conditions in the study area (Han et al., 2022; Zhang et al., 2018). In order to characterize the trade-off as the root mean squared error of each benefit, the trade-off between soil moisture and vegetation in the test plots was quantified using RMSD approach (Han et al., 2022; Wang et al., 2017). The relative benefits of soil moisture (BSM_i) and vegetation or landscape indices (VLI_i) were defined as follows:

$$BSM_i = \frac{SM_i - SM_{min}}{SM_{max} - SM_{min}} \quad (2)$$

$$VLI_i = \frac{VLI_i - VLI_{min}}{VLI_{max} - VLI_{min}} \quad (3)$$

$$RMSD_{VLI/SM,i} = \frac{BSM_i - VLI_i}{\sqrt{2}} \quad (4)$$

The calculated values of soil moisture and vegetation landscape indices in plot i are denoted as SM_i and VLI_i , respectively; the lowest and maximum values were denoted as SM_{min} and SM_{max} .

The trade-off states can be classified into three distinct categories, which are determined by the values of RSMD. Details were shown in Fig. 3.

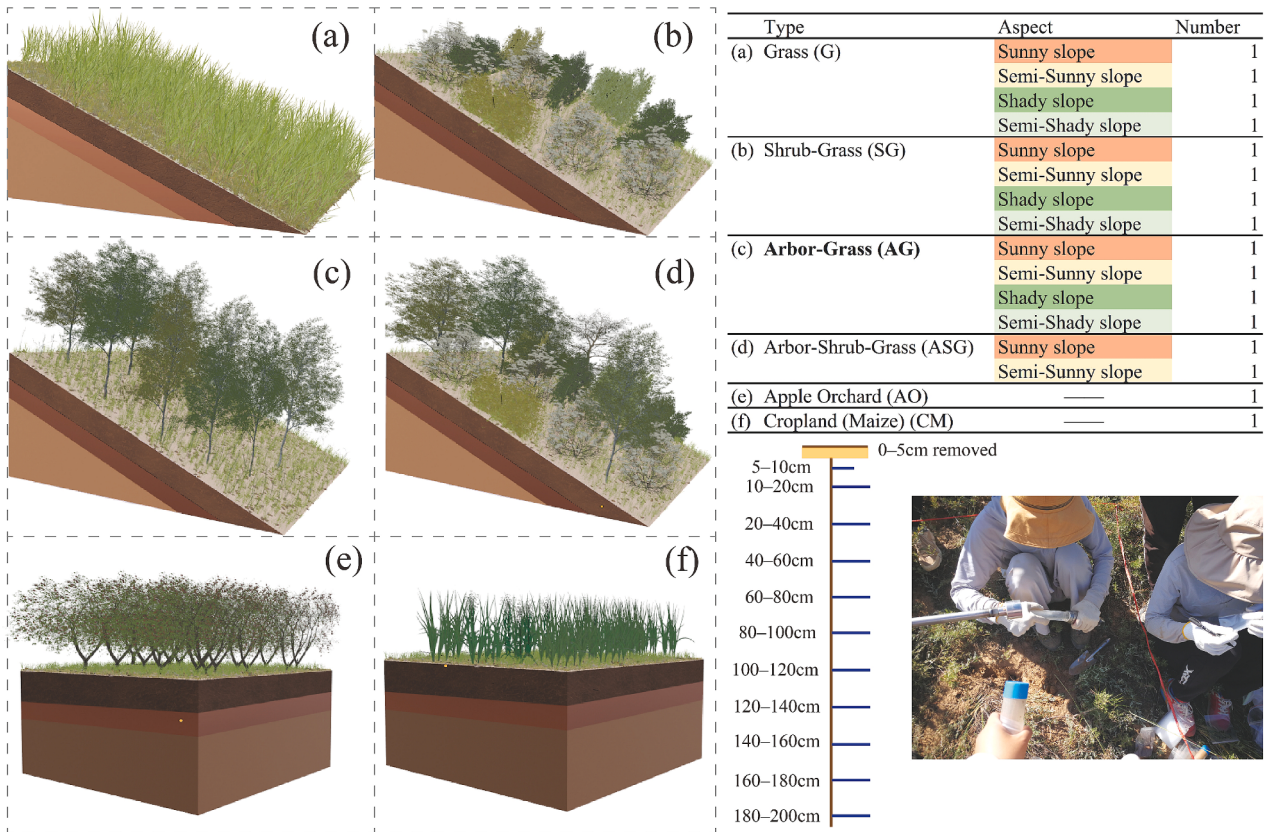


Fig. 2. Details about sampling plots (types of vegetation plots, number, and soil depth). (a)-(f) represent six types of plots (grass, shrub-grass, arbor-grass, arbor-shrub-grass, apple orchard, and cropland). Apple orchards and cornfields are agricultural land, planting in flat areas as the crop yield and the cultivation process. Some details about sampling plots are shown in the table in this figure. The scale in the figure indicates the depth at which the soil sample was taken. The photo in the lower right corner shows the field process of samples collection, using 2-meter-long stainless-steel earth auger and plastic tubes.

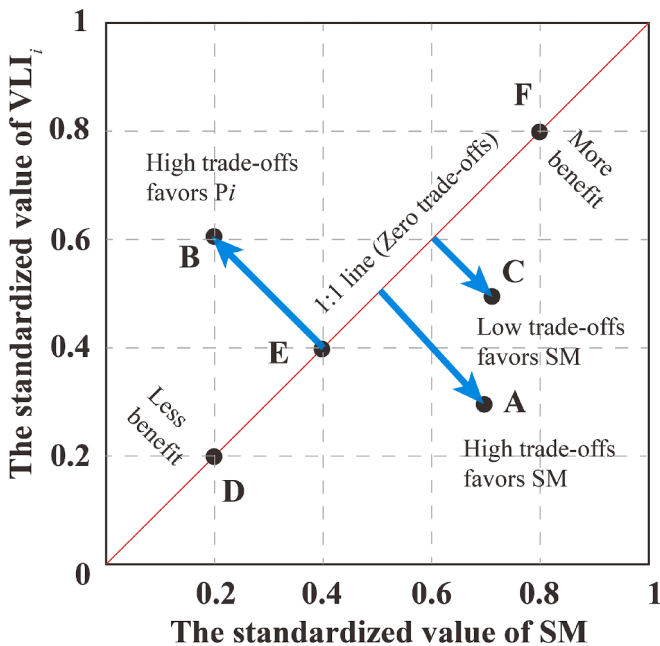


Fig. 3. Relative benefits based on root mean square deviation method.

The distance of each point to the diagonal (Su et al., 2021)—where the benefits of the two variables are equal—was used to describe the trade-off. The trade-off index increases as the distance to the diagonal increases for each variable (Bradford and D'Amato, 2012). When the

RMSD is less than 0, the soil moisture is in a state of deficit; when the RMSD is close to 0 (zero trade-off), the soil moisture can support the growth of vegetation during this period. If the RMSD is greater than 0, the soil moisture is sufficient to support the growth of vegetation in this vegetation structure of the plot.

2.4. Cubic spline interpolation

Cubic spline interpolation is a widely employed mathematical technique utilized for the purpose of generating additional data points within the range defined by a given set of known points. The aforementioned points represent the function values of an interpolation function, commonly known as a spline, which is composed of a number of cubic piecewise polynomials.

Cubic spline interpolation involves the construction of a spline $f : [x_1, x_{n+1}] \rightarrow R$ with n cubic polynomials, denoted as f_1 to f_n . A spline is a mathematical function that is defined by a collection of piecewise polynomials. In contrast to regression, the interpolation function evaluates every $n + 1$ predetermined points of a given data set D . The resulting function exhibits the following structure:

$$f(x) = \begin{cases} a_1x^3 + b_1x^2 + c_1x + d_1 & x \in [x_1, x_2] \\ a_2x^3 + b_2x^2 + c_2x + d_2 & x \in (x_2, x_3] \\ \dots \\ a_nx^3 + b_nx^2 + c_nx + d_n & x \in (x_n, x_{n+1}] \end{cases} \quad (5)$$

It should be noted that polynomials have a limited validity inside a specific interval, as they form the basis for the interpolation function. Extrapolation is a method used to forecast or estimate future values outside the observed range of data, whereas interpolation is a technique

employed to estimate values within the existing boundaries $[x_1, x_{n+1}]$ of the data. The function smoothly traverses points with suitable polynomial coefficients a_i , b_i , c_i , and d_i . The coefficients are determined by combining multiple equations into a uniquely solvable system.

2.5. Land use/land cover classification

Land use/land cover in the study area was categorized as cropland, forest, grass, orchard, construction land, economic forest, unused land, and water based on orthophotos acquired by the FEIMA ROBOTICS D200 UAV. The images pre-processed with geometric correction, aberration correction for projection, and merging were acquired at the right time with suitable sunlight. Given the influence of sunlight, to ensure the reliability of the classification results, the images were divided into four parts based on the visual color from line stretching, and then the four images were executed object-oriented classification after “polygon to raster” separately. In terms of waveband selection, the orthophoto acquired in the field includes three bands of red (R), green (G), and blue (B), and the VLI (vegetation and landscape indices) was calculated by R, G, and B bands. Therefore, the four bands were input into eCognition for classification (Costa et al., 2020). The classification results of four parts were edited for correcting types based on the actual information of the landscape. In addition, the raster with the same adjacent attributes was merged to export the LULC classification map in vector format (*.shp). For proper operation of subsequent steps, vector to raster (TIFF), in ArcGIS 10.6, is crucial to maintain the consistency of class names.

$$VI = (2G' - R' - B') - (1.4R' - G') \quad (6)$$

where, VI is a vegetation index calculated with a red band, green band, and blue band. R' , G' , B' are respectively their proportions in the sum of R , G , and B .

2.6. Landscape indices

The calculation of relevant landscape pattern indices implemented with the platform FRAGSTATS 4.2 software. The orthophoto with a spatial resolution of 0.053 m was resampled to 0.5 m for the convenience of the later calculation. In the calculation of landscape pattern indices, the LULC data were resampled to 1 m for the parameter calculation of landscape pattern scale in software with the condition that the information of data was not lost. The results were resampled for the limitation of calculation and boundary error from splitting the raster. Boundary error would result in discontinuous raster data in the study area, which was tested and verified in several runs of the program. Taking into account the similarities among landscape indices, parameters with strong characterization were selected in the first analysis. However, all landscape pattern indices were calculated in this study because of the spatial variability of the landscape indices and the regional characteristics. It was assumed that the landscape pattern is related to local soil moisture, and the landscape pattern indices combined with the sampling soil moisture data, related vegetation, and topography. Parameters that were not well characterized and redundant were excluded, and key parameters were selected for subsequent analysis in the study area. The landscape pattern indices involved in the calculation are shown in the table below (Frohn, 1997; Gergel and Turner, 2017; Lamine et al., 2018) (Table 1).

The landscape pattern indices were divided into three types from the definition that is Contagion/Interspersion (CONTAG, IJI, PLADJ, AI, LSI, COHESION), Subdivision (NP, PD, DIVISION, SPLIT, MESH), and Diversity (SHDI, SIDI, MSIDI, SHEI, SIEI, MSIEI). Among them, the larger values of CONTAG, PLADJ, AI, COHESION, MESH reflect a higher degree of landscape aggregation; the larger values of IJI, LSI, DIVISION reflect a higher degree of landscape fragmentation. The higher diversity index indicates the richer the landscape type, but dominated landscapes were demonstrated inversely; the higher the evenness index, the more

Table 1
Landscape metrics used in the present study.

Landscape Index (abbreviation)	Landscape Index (abbreviation)
Contagion (CONTAG)	Shannon's Diversity Index (SHDI)
Interspersion Juxtaposition Index (IJI)	Simpson's Diversity Index (SIDI)
Proportion of Like Adjacencies (PLADJ)	Modified Simpson's Diversity Index (MSIDI)
Aggregation Index (AI)	Shannon's Evenness Index (SHEI)
Landscape Shape Index (LSI)	Simpson's Evenness Index (SIEI)
Patch Cohesion Index (COHESION)	Modified Simpson's Evenness Index (MSIEI)
Number of Patches (NP)	Landscape Division Index (DIVISION)
Patch Density (PD)	Splitting Index (SPLIT)
Effective Mesh Size (MESH)	

evenly distributed in all landscape types, and inversely indicates that dominated landscapes. Shannon diversity and evenness indices performed well, and Simpson index is less sensitive to inferior species (Lamine et al., 2018). SPLIT index reflects the overall homogeneity of the regional landscape by the number of all patches.

3. Results

3.1. Vertical distribution characteristics of deep soil moisture

According to the division of shady-sunny slopes and vegetation cover types, the sampling plots were designed and soil samples taken in the field. The variation of soil moisture content with the depth of the soil layer in each sampling plot were shown in Fig. 4.

The soil moisture variation with depth was similar for different vegetation cover types (Fig. 4). The soil moisture content increased from 2%–5% in the surface layer (<10 cm) to 5%–12%, most fluctuating in 0–20 cm. The changes in water content with soil depth were not significant in each vegetation type from 20 cm to 200 cm, where 80 cm can be regarded as the second turning point of variation in soil moisture content.

The slope direction was divided into sunny, semi-sunny, shady, and semi-shady slopes according to the slope angle and typical geomorphological hilly and gully features. The four typical vegetation cover structures that grass, shrub-grass, arbor-grass, and arbor-shrub-grass were found both on sunny slopes and semi-sunny slopes, but the plots of arbor-shrub-grass were not present on shady slopes and semi-shady

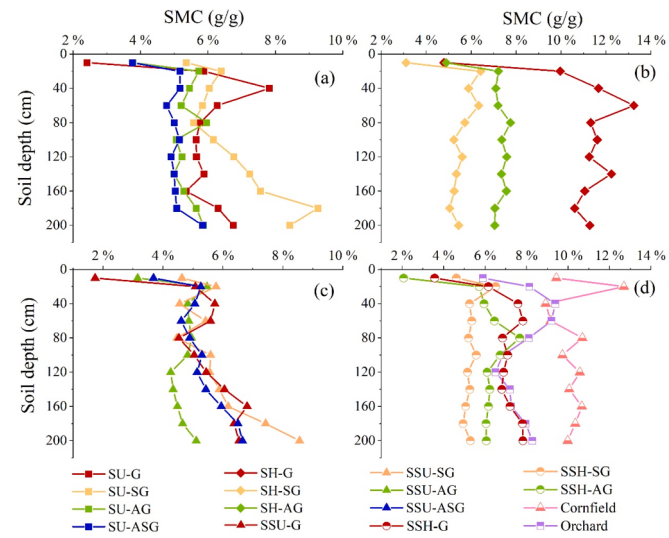


Fig. 4. Changes in soil water content with depth in typical sampling plots. Shady-slope (SH), Semi-Shady-slope (SSH), Sunny-slope (SU), and Semi-Sunny-slope (SSU); G, SG, AG, and ASG is grass, shrub-grass, arbor-grass, and arbor-shrub-grass.

slopes. The cropland (mainly cornfield) and the orchard (mainly apple orchard) are on a flat slope, not differentiating the slope direction. The relative magnitude of water content in the sampling plots varied on the soil depth. On the whole, the moisture conditions of grass and shrub-grass had more advantages on sunny slopes and semi-sunny slopes; and the moisture content of soil on shady slopes and semi-shady slopes ($G > AG > SG$) had more advantages compared with sunny slopes. All vegetation types on all slopes showed a significant increase in water conditions with soil depth in 0–20 cm. The dynamics were more stable in deeper soil layers on shady slopes and semi-shady slopes. On semi-shady slopes, the increasing trend of each vegetation cover type had significant consistency. Soil moisture on sunny slopes (sunny and semi-sunny slopes) tended to increase with soil depth below 80 cm and deep soil moisture content on semi-shady slopes showed a significant positive correlation with soil depth (SSU-AG: 0.945*, SSU-SG: 0.956*, SSU-G: 0.868*, SSU-ASG: 0.947**).

For grass plots, the surface soil water content of the grass sampling plots was relatively low, with the strongest fluctuations occurring in 0–60 cm (Δ : 3.99%–8.45%). The values of deep soil water content were higher in all slope directions of grass plots, with the maximum water content of 7.82%, 13.23%, 6.81%, and 7.83% respectively. However, a decrease of moisture content appeared in 40 cm–80 cm and 120 cm–160 cm depth layers on the SU, SSU, and SH slopes (Δ : 0.53%–2.05%), and a 0.99% decrease in 40 cm–80 cm depth on the SSH slope.

For shrub-grass plots, soil moisture was higher on sunny (5.35%), semi-sunny (4.63%), and semi-shady (4.62%) slopes than on shady slopes (3.10%) in the surface layer (<10 cm) but similar variation trend in 20 cm–80 cm for each direction. The variation of soil moisture increased with the largest growth rate under 80 cm (to 9.26%), while the soil moisture decreased by 0.81% and 0.83% at 20 cm–80 cm and 180 cm–200 cm, respectively. On semi-sunny slopes, soil moisture decreased by 1.21% and 1.06% at 20 cm–40 cm and 60 cm–80 cm, respectively. Soil moisture content increased mostly under 160 cm (6.17%) and grew up to 8.56% at 200 cm soil depth. On shady slopes and semi-shady slopes, the soil moisture varied less between 5% and 6%, and deep soil moisture did not increase significantly but less than 20 cm (−0.98%, −1.22%).

For arbor-grass plots, whose variation of soil water was similar to shrub-grass plots, the soil moisture showed a positive correlation with soil layer depth. The surface soil moisture in arbor-grass plots were 2%–4%, and the variation below 20 cm on each slope was more stable than that of grass plots. In addition, the water condition was weaker than plots of shrub growing on sunny and semi-sunny slopes but was stronger than shrub-grass plots on shady and semi-shady slopes. There were significant moisture reductions in the 80–120 cm soil layer for all slope directions, 0.73%, 0.39%, 0.63%, and 1.57%, respectively, with more stable fluctuations in the SH slope direction. Stable variations of soil water in each slope direction were in soil layers below 120 cm, 5–6%, 7–8%, 4–5%, and 6%, respectively. In detail, the water content of the deep soil layer in the SU, SH, and SSH slopes did not significantly differ from its at 20–60 cm, with “increasing first and then decreasing” at 60–120 cm in the SSH slope. But on the SSU slope, the deep soil water was less than the layer of 20–100 cm in arbor-grass sampling plots. Soil water content and variation trends, increasing with the depth of the soil layer, were similar for soil layers on sunny (3.77%–5.84%) and semi-sunny (3.68%–6.65%) slopes in arbor-shrub-grass sampling plots.

Similar fluctuations for the cropland and orchards, planted on flat plots, showed a trend of “increase and then decrease” around the 20–40 cm soil layer. Soil water content in the surface layer (<10 cm) in cropland (cornfield) was 9.43%, increasing to 12.69% at 20 cm, decreasing to 8.92% at 40 cm, and then fluctuating between 9% and 11% with depth. In apple orchards, soil water content was 5.90% in the surface layer (<10 cm), increasing to 9.20% at 60 cm, decreasing to 8.12% at 80 cm, and then fluctuating between 6% and 8.5% with depth. Overall, the soil moisture was lower in the orchard than in the cropland in this study area.

3.2. Relative benefits of VPs with deep soil moisture

The relative benefits of the vegetation parameters were calculated with the deep soil moisture at each soil layer respectively. The advantage of three-dimensional graph over the two-dimensional in fully capturing the variation of soil moisture trade-offs with layer depths. The three-dimensional trade-off state distribution of the sampling plots was plotted with Origin 2021 Pro software, and the zero trade-offs were displayed as a cubic diagonal surface (Fig. 5).

The benefits of the trade-off between vegetation restoration and soil moisture in each soil layer at the scale of sample points (sampling site) were shown in Fig. 5. The data points of each soil trade-off state are distinguished by color, and the farther the data points from the diagonal of the cube, the more they deviate from the “zero trade-off” state. If the data point located in the upper left of the cube, it indicated that the relative benefit of soil moisture in this soil layer on the sampling site was higher than that of vegetation, the trade-off condition was more favorable, and the soil moisture was in a “surplus state”. On the contrary, if the data point was closer to the lower right corner of the cube, it indicated that there was a risk of soil moisture deficit in the soil layer, and the soil moisture could not guarantee the long-term healthy growth of vegetation.

Overall, most data points were located in the lower right of the diagonal of the cube, indicating a risk of water deficit in vegetation growth in the Chaigou Watershed. Each soil layer presented different states of trade-off characteristics in the parameters, which varied in response to the trade-off state of soil moisture in different sampling plots. For example, R and Margalef indices were similar in definition (both characterizing species diversity), and the data distribution indicated similarity in characterizing trade-off benefits (Fig. 5). A distinct aggregation of data points for D₂ and E existed in the lower right corner of the cube, indicating that the data distribution exhibits a notable degree of asymmetry, indicating a large departure from the normal distribution.

The trade-off of soil water content status in each layer were calculated with different vegetation indices, respectively. The heat map of the distribution for the state of the trade-off between soil moisture and VPs for each soil layer was plotted with Origin 2021 Pro software. The original data were not normalized to preserve the original relative characteristic differences in the data for visual quantification of the trade-offs (Fig. 6).

As shown in Fig. 6, different trade-off benefits were presented for the same soil layer and same site with different vegetation indices, particularly evident at the surface layer (5 cm–10 cm) and deep soil layer (below 160 cm) in the sampling site. For example, plot 1 (SSU-SG) showed a water deficit in most indices on the surface (5 cm–10 cm) and deep soils (160 cm–180 cm), but total species indices tended to a surplus of water benefits. In plot 16 (Orchard), evenness indices had low calculated values in each layer, showing a “deficit” state; the trade-off of the other indicators was more than 0.2, showing a “surplus” state.

Plot 15 (Cropland) had better soil moisture conditions in all layers (most RSMD > 0.2), and better than other plots in this watershed. However, Fig. 6 showed that the cropland had low trade-off indices in some soil layers, such as 40 cm–60 cm and 140 cm–160 cm, at risk of deficit. Plot 9 (SH-G) had absolute dominance of soil moisture conditions in each sampling plot, where the dominance increased significantly with soil depth below 40 cm, and the soil water shown a stable state of “surplus” under 40 cm in all vegetation indices. In addition, plot 1 (SSU-SG) and plot 2 (SU-SG) showed an increase in RSMD values below 180 cm, and the superiority of soil moisture benefits. The RSMD values of the indices in plot 12 (SSH-AG) showed a general trend of being low. Furthermore, several vegetation factors demonstrated values lower than −0.5 especially in the deep soil layers. These findings suggest that the soil moisture benefit in this watershed was insufficient, with a heightened chance of experiencing soil moisture deficit.

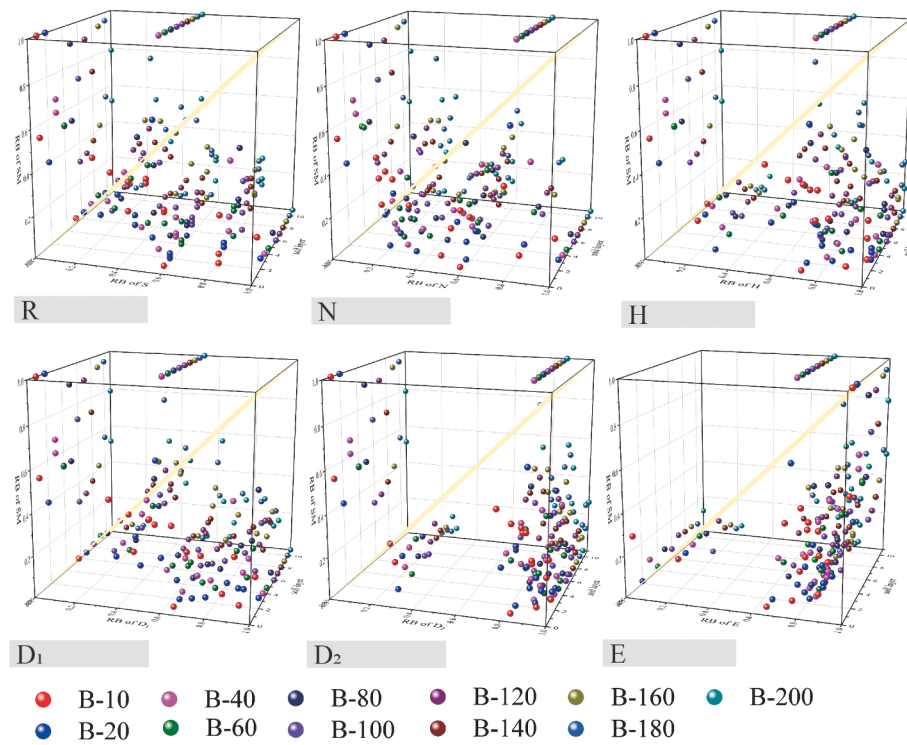


Fig. 5. Vegetation indices and relative soil moisture benefits of each soil layer. B-10, B-20, and B-40 represented the BSM in the 5–10 cm, 10–20 cm, and 20–40 cm soil layers, respectively, the same for other soil layers. The coordinate system was right-handed; the X and Z axis were BSM and BVLI, respectively, and the Y axis was the depth of the soil layer.

3.3. Regression analysis of trade-offs in three-dimension

The independent variable was set as soil moisture content (%), variable Y was set as soil depth (cm), and variable Z was set as the trade-off index (RSMD) to construct a three-dimensional scatter plot of the right-hand coordinate system in consideration of the data dimension and the rationality of scientific analysis (Fig. 7). Certain requirements were needed for data smoothing of the fitted model because of the poor linear characteristics of the field sampling data but strong grouping characteristics. As the ordinary linear regression was difficult to meet the fitting requirements of the data, the LOWESS local regression was performed to fit the 3D surface in MATLAB R2017a software (Fig. 7).

In the fits of many parameters, Margalef diversity index at the sampling site scale had the highest fitting accuracy ($R^2 = 0.7465$), followed by R ($R^2 = 0.7363$), as shown in Fig. 7. Moreover, the fitting effect of Shannon index (H) in the sampling area was also quite effective with $R^2 > 0.6$. But the worst fitting effect was evenness with an R^2 of only 0.3841.

Through the fitting of soil moisture trade-off conditions, the inflection points of soil moisture trade-off in sustaining vegetation growth for a given year were derived. The data points of each parameter were concentrated around 4–8 % soil moisture content, and they showed approximately the same trend as the fitted surfaces. In detail, soil moisture content, 7.5–8.5 % approximately, was the trend turns of the trade-offs while the surface turns occurred around 9 % of the diversity indices (H, D₁ & D₂) at the sampling site scale. Except for the D₂ (9 %) and E (11 %), the zero trade-off inflection points for the other parameters were in the vicinity of 7–8.5 % soil moisture content. No significant fluctuation of the fitted surface in the Y-axis for each parameter, but local liftings of the surface were apparent when the soil depth (Y) was over 140 cm. R, H and D₁ indices were well fitted, with a larger surface tilt compared to other poorly fitted parameters, where the values of the former three trade-offs ranged from –1 to 1. With low dispersion in the Z-axis, the data points were arranged in the data concentration zone,

close to the fitted surface. R, H and D₁ with data concentration ranges, inflection points, and trend inflection points of zero trade-off were shown in Table 2.

The zero trade-off inflection points for R, H and D₁ were all around 8 % (soil moisture content) (Table 2). The same range of data sets for R and H (5–8 %), and the same trend inflection point for H and D₁, i.e., when the soil moisture content reaches 9 %, a trend turning of trade-off appeared. In general, the trade-off inflection points between soil moisture and VPs (effective) for typical sampling plots was around 8 %, and the trend inflection point was 8 %–9% in the study region.

Utilizing the cubic convolution interpolation in spatial interpolation, the surface fitting of data can be enhanced in MATLAB 2017 software to align with the model of soil moisture trade-off benefits. This facilitates the identification of the inflection points in the transition of trade-off status and enables the incorporation of additional characteristic information pertaining to vegetation restoration at the sampled location. The initial findings from the local regressions indicate that the Margalef, Shannon-Wiener and Richness effectively capture and represent the trade-off in soil water in the revegetation site (Fig. 8). Therefore, an investigation was conducted into the utilization of local regression and interpolation modeling methods for the analysis of these three indices. The results suggested that the cubic convolution interpolation exhibited superior fitting accuracy compared to other approaches. Additionally, it effectively captured the local soil water balance and accurately represented the surface fitting trend. The model computation given in this study provides a more precise representation of the trade-off state observed in typical areas of plant restoration in three-dimensional spatial surface.

The cubic convolution interpolation process results in a surface that is in a fully fitted state, leading to an R^2 value of 1. This indicates that the fitting effect is superior to that of simple linear regression and optimized nonlinear regression methods, particularly for three-dimensional fitting. Additionally, cubic convolution interpolation demonstrates better applicability in this scenario. The cubic convolution interpolation

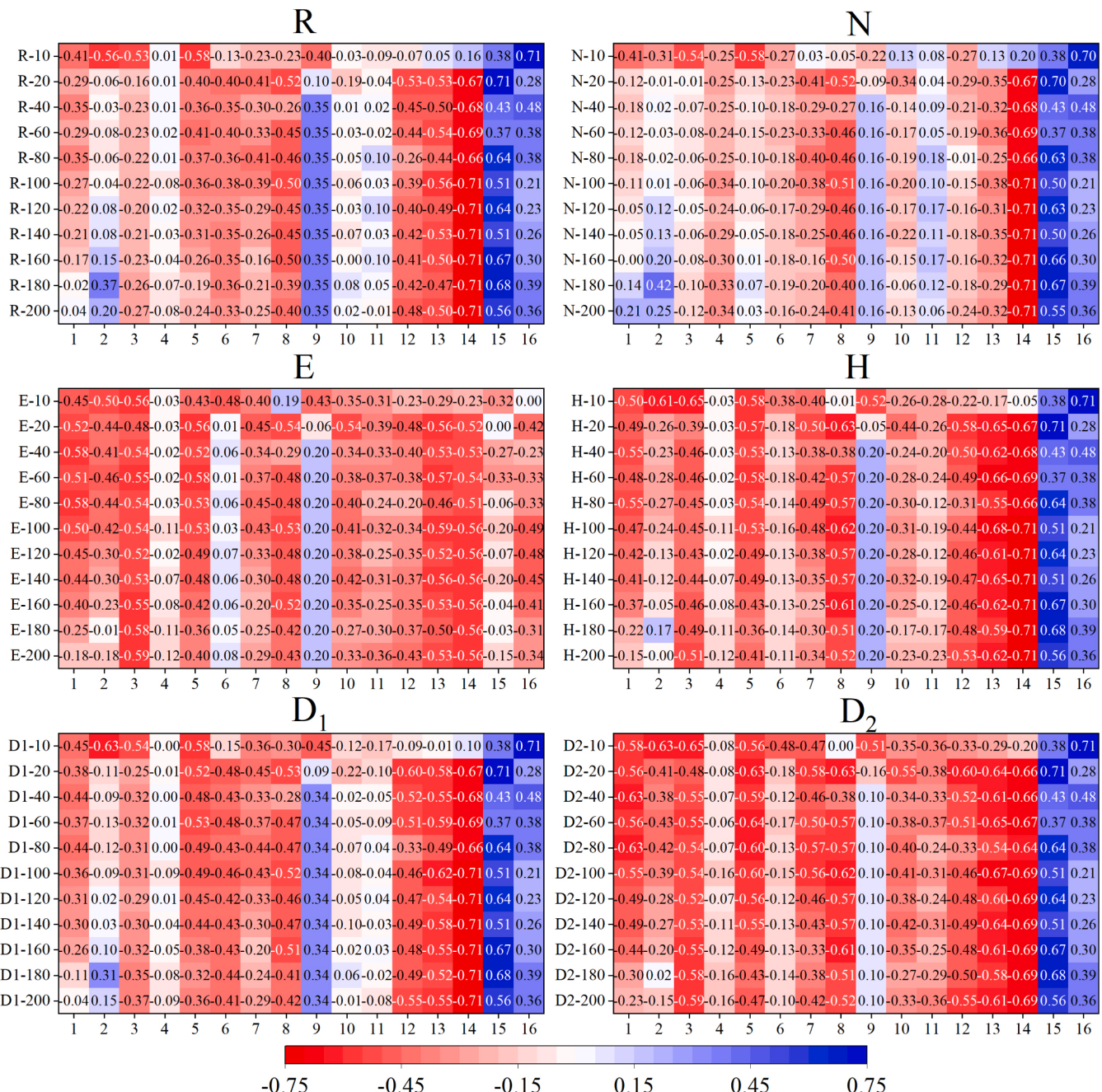


Fig. 6. The heat map for the trade-off of soil water in each layer. The x-axis represented the 16 sampling plots (1–16: SSU-SG, SU-SG, SSH-SG, SH-SG, SSU-ASG, SU-ASG, SSU-G, SU-G, SH-G, SSH-G, SH-AG, SSH-AG, SU-AG, SSU-AG, Cropland and Orchard), and the y-axis represented the depth of soil layers, for example, R-10 is 5 cm–10 cm, R-20 is 10 cm–20 cm, and R-40 is 5 cm–10 cm.

method demonstrates superior performance in terms of fitting accuracy across all parameters within the available model fitting options. Among the three indices examined, the spatial interpolation fit exhibits similar overall trends and spatial divergence in the alteration of trade-off status. However, it is the Shannon index that outperforms the others, as evidenced by its lower SSE value. Furthermore, the Shannon index demonstrates a more straightforward spatial interpolation effect, as depicted in the projection plot at the right section.

The soil moisture state of each soil layer can be visually represented through the utilization of a bottom projection diagram, which effectively illustrates the observed pattern of variations. As depicted in Fig. 8, the moisture content of the lower soil layers exceeds 4.5 percent. Moreover, the association between deeper soil moisture and surface land

cover shows a relatively modest variability, characterized by a “trapezoidal” pattern in terms of deeper soil moisture and water trade-off status. The occurrence of trade-off state inflection points, also known as zero trade-off inflection points, can be observed in sections that are colored green and blue-green. The first group of inflection points, indicating a transition from deficit to surplus, exhibits a rightward and leftward shift as soil depth increases, approximately distributed throughout the range of 7.5–8.5 percent. The inflection points of the second group, indicating a transition from a favorable to an unfavorable trade-off, exhibit a rightward and then leftward shift. In the case of shallow soils (with a depth of less than 40 cm), a deficit condition arises when soil moisture has not yet reached the desired level but is around 10 percent. Under similar moisture conditions, namely ranging from 6 to 8

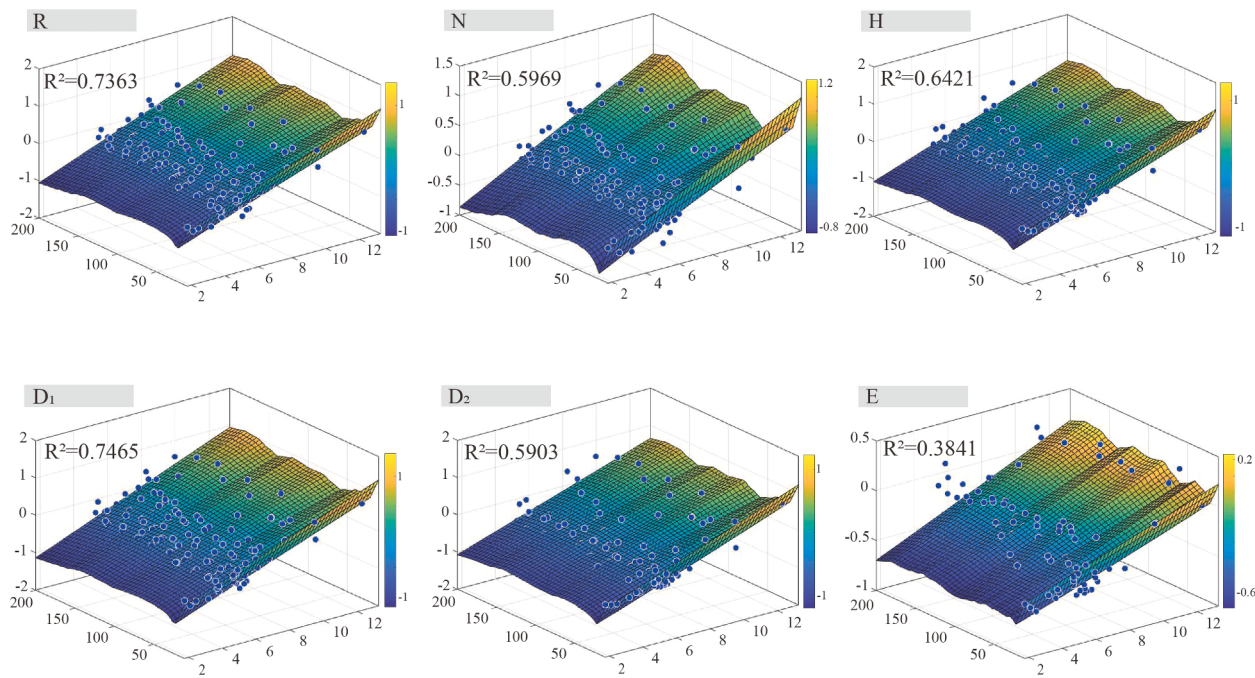


Fig. 7. The trade-off between soil water and VPs with local weighted regression. The X-axis was set as soil moisture content (%), Y-axis was set as soil depth (cm), and Z-axis was set as the trade-off index (RSMD).

Table 2
Surface fitting characteristics of R, H and D₁.

Data set range	Zero trade-off inflection point	Trend inflection point
R	5–8	8
H	5–8	9
D ₁	4.5–8	9

Note: inflection point represented the soil moisture content (%).

percent, it was seen that the level of soil water at depths between 50 and 120 cm exhibited a comparatively superior performance compared to other depths. However, it is important to note that even at these depths, the soil water was still considered to be insufficient. The soil water trade-off for same soil layers exhibits a pattern of initial increase followed by decrease, resulting in an overall positive increase, when the water content was 7–12 percent. The occurrence of the second group inflection points (below 50 cm) was early in shallower soil layers.

3.4. Land use/land cover classification based on orthophoto

The orthophoto data of the Chaigou Watershed was obtained by UAV image correcting and stitching. The land use was classified into nine categories in the study area combined with the geomorphology, surface cover characteristics, and the research theme. The segmentation scale was designed as 10 after tested, and the point selection in the high-resolution image with field sampling data were helped for accuracy evaluation. The confusion matrix and kappa coefficient were used to evaluate the accuracy of land use classification with ArcGIS and Excel software. The spatial distribution of land use/land cover in the Chaigou Watershed is shown in Fig. 9. The overall accuracy was 0.918 and the kappa was 0.878 (>0.85), which indicated that the classification results satisfied to describe the surface land use cover information.

The dominant land use type was grassland (27.799 km²) with 45.9 % under vegetation restoration in the Chaigou Watershed, which was followed by forest (21.212 km², 35 %) and unused land (6.292 km², 10.4 %). Economic forests (3.2 %), cropland (2.8 %), and orchards (1.9 %) account for a relatively little proportion of the area, while

construction land was 0.536 km² and water was the least (2711 m²). In terms of spatial distribution, grassland, and forest were alternately distributed, which was closely related to the topographic relief and shady slope direction. A northwest (gully head)-southeast alignment was in this area, with significant spatially divergent features as land use/cover types bounded by flowing branches. Because of similar surface exposure, the silt dam was regarded as unused land in the classification and interpretation, mainly located on the southwest side of the gully, where the slope direction was at the junction of the semi-sunny slopes and semi-shady slopes. DEM data showed that economic forests, orchards, and cropland tended to be interphase distribution in higher terrain. The economic forest (planted with a regular shape and distinctive texture in the image) was mainly distributed on the southwest side and also on the northeast side, with a “scattered but even in spatial” distribution feature. The orchards are more concentrated on the higher ground on the east side of the gully, and scattered on the southeast side of the watershed.

Besides, the distribution of orchards concentrated in the higher terrain on the east side of the gully and scattered on the southeast side of the watershed. The cropland concentrated in the higher terrain in the northern part of the watershed, showing the characteristics of large patches, and scattered in the southern part. The area of construction land only accounts for 0.9 %, mainly including roads at higher terrain around the gully, oil production sites in the south and west of the watershed, and scattered rural residential areas. For the water area, the study area is located in a semi-arid region, where precipitation is scarce, and the sampling time requires no recent rainfall. So, there was no tributary or surface water storage. High-precision image showed that a little surface water (2711 m²) exists at the end of the tributaries in the southern gully, whose proportion was approximately equal to zero, but was not shown in the pie chart.

3.5. Calculation of landscape indices

The land use data obtained from the object-oriented method was used to calculate and analyze the landscape pattern in Fragstats 4.2 software. NP, PD, DIVISION, SPLIT, MESH, IJI, PLADJ, AI, LSI, and COHENSION were selected for landscape level calculation, for

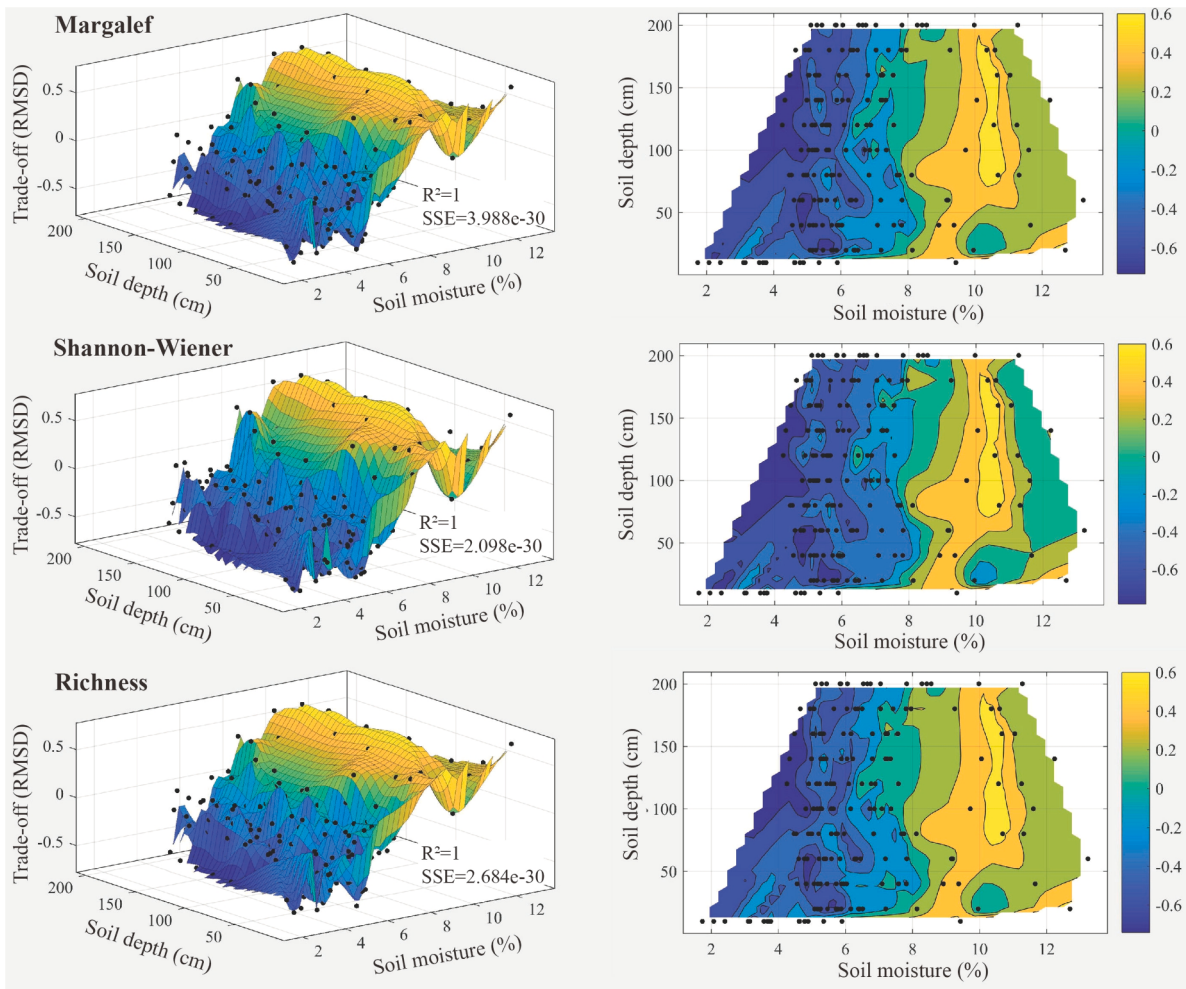


Fig. 8. Determining optimal soil moisture trade-offs by the application of cubic convolutional spatial interpolation for vegetation parameters.

evaluating the aggregation and dispersion of patches, in respect of the definition of landscape indices and the applicability in this region. The landscape-level calculation also chose SHDI, SIDI, MSIDI, SHEI, SIEI, and MSIEI.

The general calculation of landscape pattern indices was for all patches of all land classes in the study area. The values were shown in Table 3, with a total number of patches of 140,111 and a patch density of 9247.465. The CONTAG was defined as the characteristics of clustering and spreading among the individual patch types with a value of 57.028. The three diversity and evenness indices indicated that the richness of patches was not high, but the evenness indices were all over 0.5. Moreover, the other indices of subdivision and contagion/interspersion values were similar to the grass.

The moving window method was used to explore the spatial distribution characteristics of landscape patterns within the study area. Since the spatial differentiation characteristics of the landscape pattern indices were strongly regional, the 17 parameters contained in the subdivision, Contagion/Interspersion, and Diversity indices were all involved in the calculation (Fig. 10). As the data source of the study area was high-precision orthophoto data, the number of data raster rows was beyond the range of the software operation, and it could not be used after raster segmentation due to the edge effect, so the full raster input was needed to ensure the data results. An attempt was made to find that the data accuracy of 0.5 m resolution (the same spatial accuracy used for land use classification) did not meet the data running conditions. For that reason, the raster data were resampled to 1 m to ensure that the data running and spatial scale analysis requirements were met. The spatial

distribution of the landscape indices in the Chraigou Watershed calculated with the moving window method was shown in Fig. 10.

As shown in Fig. 10, there was a spatial correlation in landscape pattern indices, such as NP-PD, PLADJ-AI-LSI, etc. The spatial heterogeneity of SPLIT indices was weak, and the range of values was narrow in most of the study area. The characteristics of the spatial divergence were similar for the three kinds of diversity and evenness indices, and one of them would be taken in the subsequent research. Regarding the land types, the landscape pattern indices were regionally consistent with the land use/cover distribution. The distribution of forest and grassland was more scattered but homogeneous, and the landscape pattern indices of bare land (silt dam) with concentrated patches were significantly variable compared with other surrounding land types. The construction land (surrounding roads) was assigned a null value, and the spatial patch characteristics of orchards, economic forests, and cultivated land varied according to the indices.

As the landscape pattern indices responded to the degree of aggregation and division of patches, both meanings and operations of the parameters led to different degrees of data redundancy and correlation among the selected factors. Effective and representative parameters of the study area were selected to eliminate redundant information and to provide a guide for the selection of factors for following trade-off calculations. With the R Studio packages “terra”, “Hmisc”, “Performance Analytics” and “GGally”, correlations between the various parametric layers were calculated and the significance analysis was displayed in Fig. 11.

As shown in Fig. 11, the landscape indices were all significantly

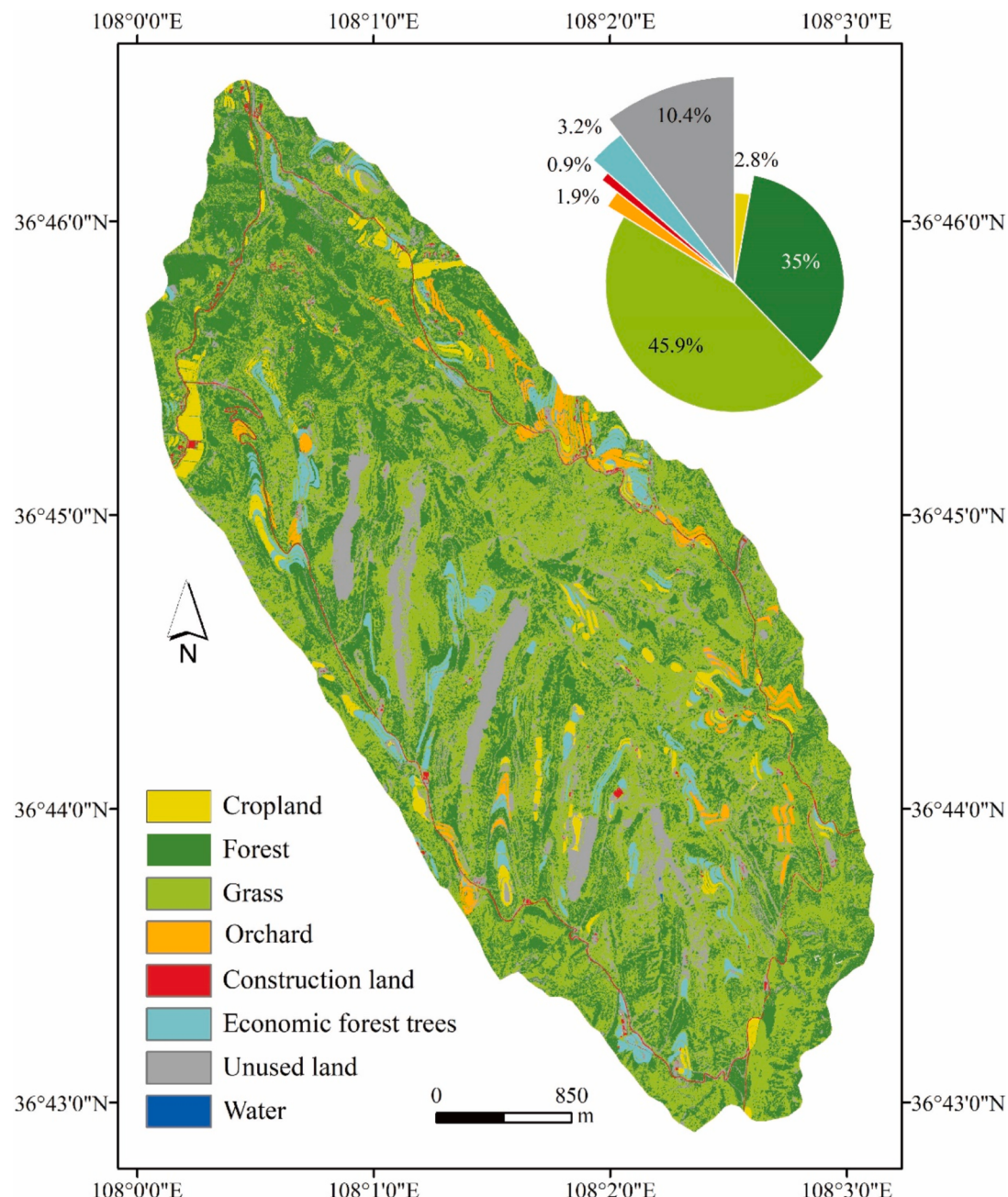


Fig. 9. The typical sample plots in the study area and land-use/land-cover (LULC) for measuring vegetation and soil water in the Chaigou Watershed of the CLP. Eight types of LULC and percentages were obtained from the object-oriented method.

Table 3
Landscape pattern index in landscape level in Chaigou Watershed.

Subdivision	NP	PD	DIVISION	SPLIT	MESH
	140,111	9247.465	0.9418	17.1746	88.219
Contagion/Interspersion	CONTAG	IJI	PLADJ	AI	LSI
	57.028	36.5495	85.8767	85.9251	275.936
Diversity/Evenness	SHDI	SIDI	MSIDI	SHEI	SIEI
	1.2866	0.6541	1.0615	0.6187	0.7475
					0.5105

correlated with each other at the 0.001 level. In particular, AI was significantly positively correlated with PLADJ, NP with PD (1.000^{***}), while AI was significantly negatively correlated with LSI, PLADJ with LSI, and DIVISION with MESH (-1.000^{***}). The correlations of PD, PLADJ, and IJI with the other parameters were lower (<0.5). The fitted

curves in Fig. 11 indicated that there was a significant power-exponential relationship between similar diversity and the evenness indices, and the non-linear positive/negative correlation between the other parameters was also present. The 17 landscape pattern parameters were divided into groups according to positive and negative correlations

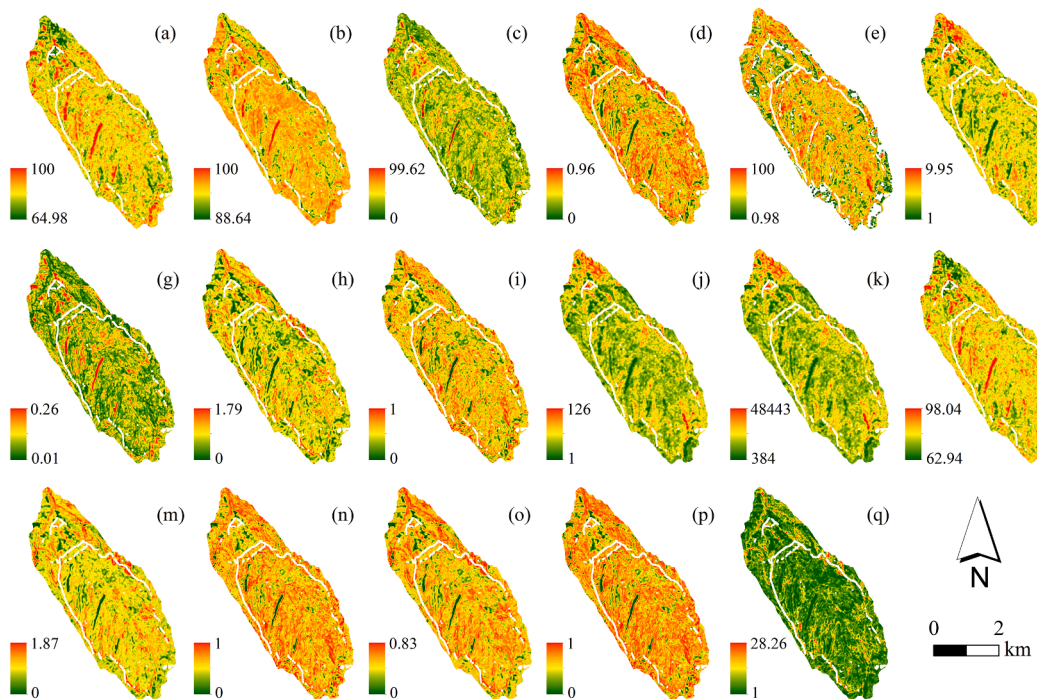


Fig. 10. Spatial distribution of landscape-level indices in the Chaigou Watershed. Note: a–q: AI, COHESION, CONTAG, DIVISION, IJI, LSI, MESH, MSIDI, MSIEI, NP, PD, PLADJ, SHDI, SHEI, SIDI, SIEI, SPLIT.

to facilitate subsequent trade-off benefit analysis. Where A (AI)-C (CONTAG)-G (MESH)-L (PLADJ) was one group and the rest was the other group, and the parameters showed a negative correlation with each other in one group.

3.6. Trade-offs of landscape parameters

The parameter values were extracted from the sampling points determined by the raster data of landscape pattern. Among all the landscape pattern parameters, the parameters of COHESION and CONTAG demonstrated superior fitting, as evidenced by the fitted R^2 value exceeding 0.6 (Fig. 12). Also, a cubic convolutional interpolation methodology for spatial surface was applied to achieve three-dimensional surface (Fig. 13).

From the data presented in Fig. 12, it is evident that the COHESION and CONTAG indices exhibit fitting accuracies beyond 0.6, and R^2 were 0.7108 and 0.6204, respectively. The evidence of COHESION and CONTAG was demonstrated in Table 4, which included data on concentration ranges, inflection points, and trend inflection points with zero trade-off. The inflection points for CONTAG with zero trade-off were observed at approximately 8 % soil moisture content (Table 4). When the soil moisture content reaches 9 %, the inflection points of trade-off trend appeared for both CONTAG and D₁ data sets, which have the same range of 4.5–8 %. Overall, the inflection points representing the trade-off between soil moisture and landscape indices (effective) for standard sampling plots ranged from 6 % to 8 %. Also, the inflection points indicating the trend were within the range of 7.5 % to 8.5 % in the research region.

Among the several options available for models, it was observed that the cubic convolutional interpolation exhibited the most optimal method for each landscape parameter. There was a notable divergence in the overall pattern and spatial variation of trade-off conditions seen in the spatial interpolation. In particular, the COHESION index exhibited a more consistent result, whereas the CONTAG yielded lower values of SSE. The soil water trade-off condition in each soil layer can be visually represented through the graph of projection. As depicted in Fig. 13, the moisture content of the deepest soil layer exceeds 5 %. The correlation

between deep soil moisture and surface land cover exhibits a rather slight connection, while the deep soil moisture and trade-off status also demonstrate a “trapezoidal” pattern. The first occurrence of the trade-off inflection point (zero trade-off inflection point) is shown in green.

The COHESION index exhibits a beginning inflection points those transitions from a state of deficit to surplus. This inflection point demonstrates a shifting pattern, first to the right, then to the left, and subsequently to the right again, as soil depth increases. The overall trend follows a “S” shape, occurring approximately within the range of 7.5–9 % soil moisture content. The second group of inflection points were found in the 50 cm soil layer. When the moisture conditions remain consistent at a range of 8 % to 10 %, the trade-off of soil moisture is found to be more favorable at a depth of 80–100 cm compared to other depths. The soil water trade-off inside a given soil layer exhibited a pattern of initially declining and subsequently increasing, with a notable overall rise of 5 percent. This trend was observed as the moisture content within the soil layer increased within the range of 7.5 to 12 percent.

In the setting of the CONTAG index, it is observed that the initial inflection point is delayed in shallow soils as the thickness of the soil layer grows. The occurrence of the second inflection point appears subsequent to a soil depth of 9.5 percent, and is further pronounced in deeper soil layers. When moisture conditions remain the same, the trade-off of soil moisture at depths of 100–160 cm is superior compared to other layers of soil. Within a single soil stratum, the trade-offs pertaining to soil water exhibited a discernible pattern characterized by an initial increase, followed by a subsequent decrease, and ultimately an overall increase, as the water content increased. Nevertheless, it should be noted that the CONTAG index lacks smoothness and does not exhibit a spatial distribution of water trade-offs as well as the COHESION index. This can be attributed to the less effective interpolation method employed by the CONTAG index, which fails to accurately capture the distinctive features of soil water trade-offs.

4. Discussion

In sampling plots throughout vegetation restoration, soil moisture (SM) changed dramatically with precipitation and topography,

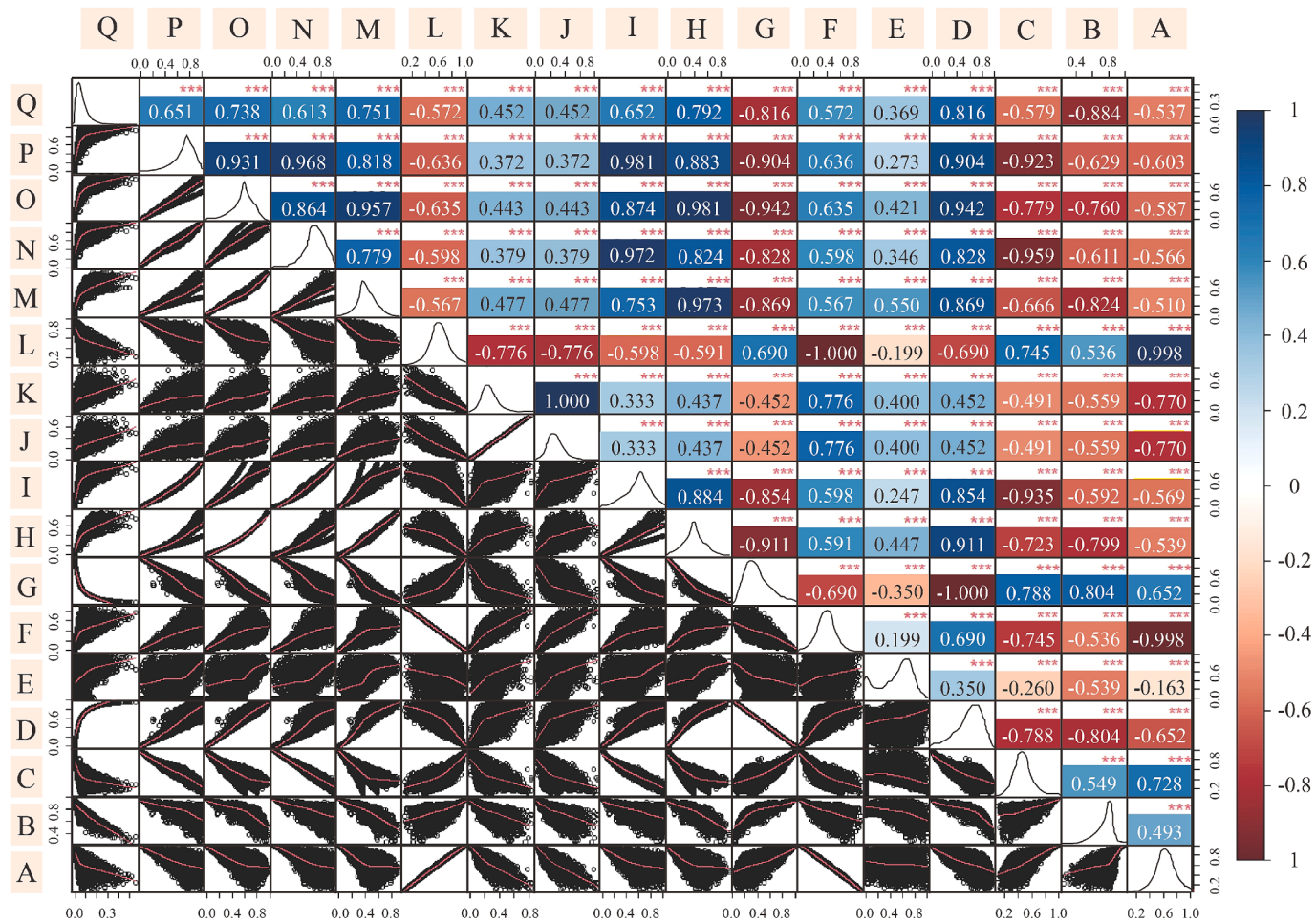


Fig. 11. Correlation and significance heat map of landscape patterns indices. Note: A–Q: AI, COHESION, CONTAG, DIVISION, IJI, LSI, MESH, MSIDI, MSIEI, NP, PD, PLADJ, SHDI, SHEI, SIDI, SIEI, SPLIT.

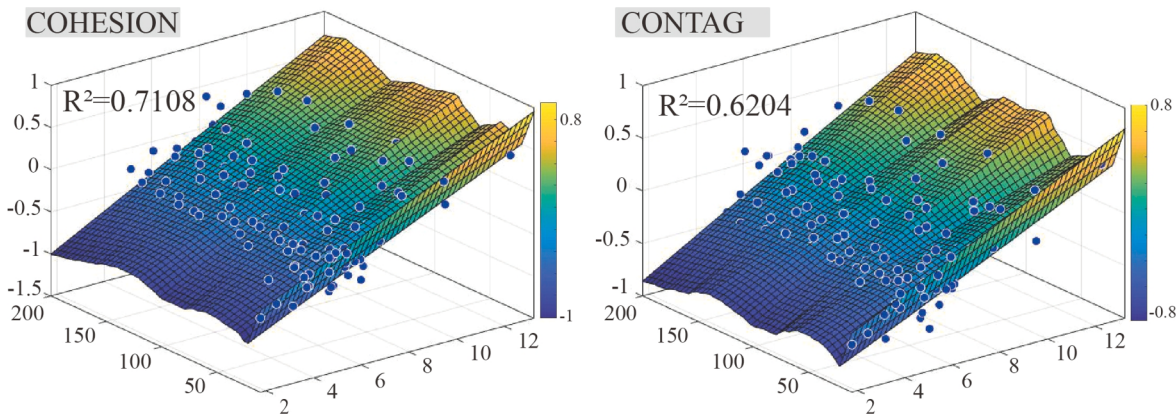


Fig. 12. The trade-off between soil water and landscape indices with local weighted regression. The X-axis was set as soil moisture content (%), Y-axis was set as soil depth (cm), and Z-axis was set as the trade-off index (RSMD).

supporting planting based on excessive soil water consumption (Fig. 4), whereas ridiculous planting was unable to maintain sustainable development of revegetation. The previous research conducted by our team has shown that the piecewise linear regression (PLQ) and nonparametric conditional quantile regression (NCQR) models are effective tools for simulating and assessing the soil water ecological status by the trade-off (Han et al., 2022).

Gradient change was in each vegetation and slope type with the

deepening of the soil layer in the Chaigou Watershed. The rational and accurate land cover classification was achieved by low-altitude orthophotography in the restored vegetation area. For the first time, the raster data information ($1 \text{ m} \times 1 \text{ m}$) of VLI was combined with the soil moisture trade-off in the sampling scale, where multiple landscape pattern indices and unit size of plots were calculated according to the classification and sampling. Each VLI showed different effects of the trade-off state, where the Margalef index had the highest surface fitting accuracy, followed by

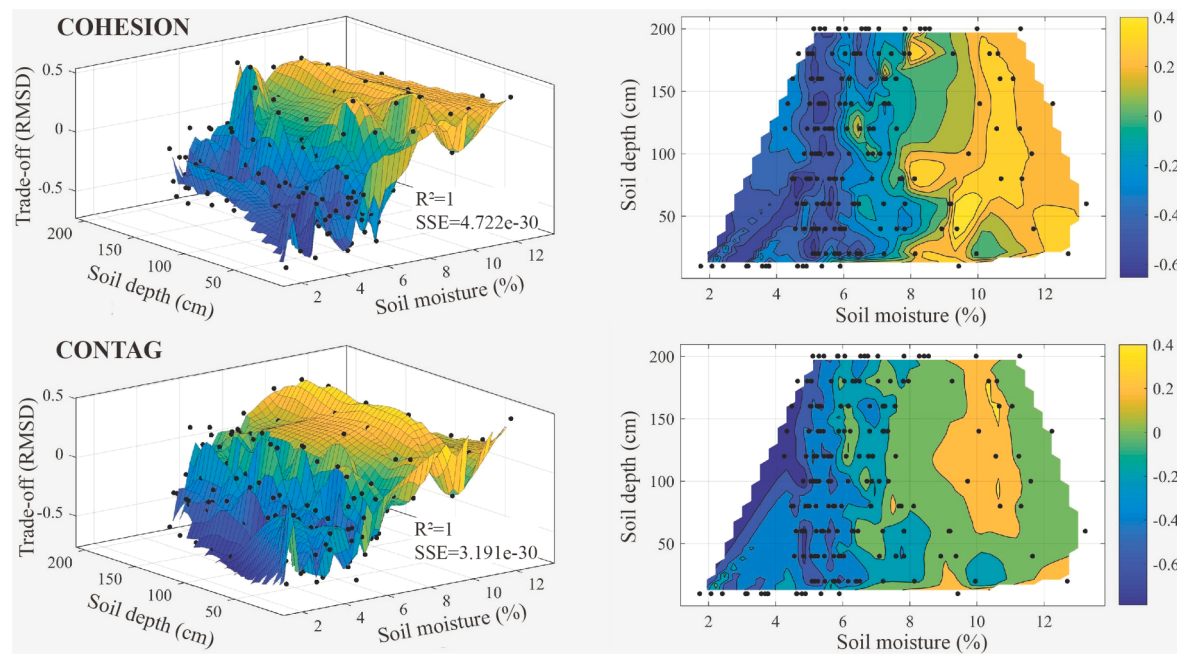


Fig. 13. Determining optimal soil moisture trade-offs by the application of cubic convolutional spatial interpolation for landscape indices.

Table 4
Surface fitting characteristics of COHESION and CONTAG.

	Data set range	Zero trade-off inflection point	Trend inflection point
COHESION	4.5–7.5	6	8.5
CONTAG	4.5–8	8	7.5

Note: inflection point represented the soil moisture content (%).

R and COHESION, while the worst fitting effect was in SPLIT index.

4.1. Vertical distribution of soil moisture in the sampling plots

According to the study, a risk of a “dried soil layer” in the revegetation plots on each slope direction was suggested by a “fold-back” phenomenon, that is, the moisture decreases significantly with the deepening of the soil layer in the typical sampling sites. Shallow soil moisture tends to promote plant growth and retain surface moisture, while deeper soil moisture contributes to root development and long-term water storage, and generally provides plant support during dry periods and maintains the ecological balance of the soil (Jia and Shao, 2014; Tong et al., 2020). In the case of grassland, for example, significant moisture reductions (Δ : 0.53 %–2.05 %) were at 40 cm–80 cm and 120 cm–160 cm, while in shrub-grass plots, soil moisture was reduced by 0.81 % and 0.83 % at 20 cm–80 cm and 180 cm–200 cm, respectively.

Given evaporation and infiltration, rapid evaporation and less soil water were in the surface layer of grass sampling plots, largest fluctuation in 0–60 cm (Δ : 3.99 %–8.45 %), where less vegetation covering. Although the cropland and orchard only had low surface soil moisture content, a risk of “dried soil layer” were still in the two types of land use/cover because of evaporation, irrigation, and water infiltration. At 20–40 cm, the cropland and orchard showed a trend of “increasing then decreasing”, and the soil moisture fluctuated between 9 %–11 % and 6 %–8.5 % with the deepening of the soil layer, respectively. But the soil moisture content of the orchard was lower than that of the cropland. It is worthwhile to explore the long-term suitability of soil moisture for two planted in the vegetation restoration area, which can provide scientific guidance for the reasonable configuration of revegetation in the subsequent vegetation restoration process. In the process of vegetation

restoration and succession, shrubs on shady and semi-shady slopes were blocked by trees from getting sufficient sunlight and failed to grow healthily; while on sunny and semi-sunny slopes, there were a few shrubs in the spaces where trees were growing because of more sunlight.

4.2. Object-oriented land cover classification

The accuracy of the object-oriented classification results with the kappa coefficient of 0.878 met the conditions, and the land use and land cover types were effectively classified reflecting the real cover conditions. However, the classification process was prone to ambiguity in the classification of unused land, grassland, sparse woodland, and small patches like meta-area refineries and other construction sites due to sparse vegetation cover, fine local patches, and the effects of aerial photography light. Furthermore, false division of raster cells was not easily found in the cropland, orchard, and economic forest as a result of textural features, aggregation, and clear boundaries. Few mis-segmentation results occurred easily between orchards and economic forests because of the membrane covering of orchards. Refinement of the segmentation of local fine pixels is necessary for subsequent studies from suitable segmentation scales. In terms of vegetation index calculation, more calculation of variable vegetation indices by multiple bands to explore their applicability in subsequent research on land cover classification (Guo et al., 2021; Yan et al., 2019). In addition, combining multi-source remote sensing data for extraction of surface vegetation structure in subsequent studies could be achieved to solve the problem of bushes restricted extraction due to the shade of trees.

4.3. Landscape parameters

To ensure the comprehensiveness and rationality of parameter selection and analysis, two kinds of landscape pattern parameters were selected for calculation and assessing the degree of patch aggregation and division around the land units based on scientific research and regional data. Grassland, forest, and unused land had large areas and many patches, especially similar contagion and division landscape indices to those of the grassland category (SPLIT, IJI, PLADJ, and AI). Grasslands were particularly prone to a high concentration of patches so they had a clear advantage over other land types in terms of patch

density and shape index. The different landscape pattern indices show slight differences in discrete aggregation characteristics, influenced by patch area, patch edge perimeter, intra-patch, and inter-patch.

The raster data were resampled to 1 m after several attempts to calculate the spatial distribution of landscape pattern indices in the watershed, to simultaneously satisfy the needs of program operation and ensure the significance of scientific research. The spatial heterogeneity of the SPLIT index was weaker than others, which was not helpful for the exploration of spatial heterogeneity. The construction land (surrounding roads) was given null values due to the influence of the calculation formula, variable range restrictions, and calculation conditions. Principal component analysis was used to eliminate redundant information as data redundancy among the landscape pattern parameters, but the principal component had low fitting accuracy. It was suggested that the unique factor characteristic information was significant in the trade-off analysis, which can be hidden by the synthesized principal component. However, overall correlation tends to ignore the local irrelevant information, and subsequent studies need to set up local correlation calculation analysis to select landscape pattern parameters with more applicability to the research.

4.4. Trade-off analysis

In this work, the trade-off between soil moisture and VLI in a typical watershed of the Loess Plateau revegetation area was analyzed by a three-dimensional cubic model with local regression surface fitting for soil moisture, VLI, and trade-offs. Although the data layout for parameters with similar meanings was resembling, differences remained between sample-scale and raster-scale data in their representational implications and neighborhood analysis, as shown by the characteristics of VLI and soil moisture trade-off conditions. So, appropriate indices should be selected in subsequent studies, according to the needs of the study content and methodology.

The total number of species was of lower reference value in for trade-off analysis depending on the heat map and all indices. Insignificant variation of trade-off was in cropland and orchard by soil layer, influenced by irrigation, but also varied by different indices. The best status of trade-off was in grass plots on shady slopes as lower water demand for grass growing than in arbor plots, while the arbor-grass plots absorbed more water with poor ecological benefits especially in deep soil layer. A clear advantage was in the deep soil layer on the sunny slope with the heavy surface evaporation of radiation.

The 3D regression model of trade-off was made because different soil layers could not be set on a two-dimensional regression model, and the data points of soil moisture content were concentrated around 4–8 %. For landscape pattern indices, some were not rational for the trade-off analysis of soil water from the fitting results, such as poor spatial heterogeneity and following low accuracy ($R^2 = 0.271$) of SPLIT. So, the subsequent study needs to evaluate the landscape pattern parameters fully and select the appropriate ones for subsequent exploration. As an example, the corresponding indices should be selected according to the various characteristics of soil moisture with depth in the sampling sites, with the guarantee of fitting accuracy, to avoid the over-aggregation of data points due to improper indices selection. The study proved that the Shannon-Wiener index (H) and Margalef index have been considered for trade-offs between soil moisture and revegetation, based on the regional representativeness of the study area and the fitting models.

5. Conclusion

In order to select suitable vegetation parameters for soil moisture trade-off assessment, this study fully considered the characteristics of the data and selected appropriate fitting models and algorithms. Precipitation, topography, and plant diversity were fully considered when analyzing the trade-off mechanisms of soil water in nonparametric models and three-dimensional analysis, which realized the development

from two-dimensional models fitting to the three-dimensional in this research field. This study also combined field sampling data with high-precision raster data and assessed the validity and stability of the models.

The trade-offs between soil moisture and vegetation restoration in each soil layer in the Chaigou Watershed were evaluated with the typical vegetation sampling and UAV image data integrated with various landscape pattern indices. The orthophotography from UAV assisted to realize the high-precision monitoring of the ecological environment in the watershed. It was found that soil moisture varied with depth and showed different patterns based on slope direction. The “fold-back” of data with terrible trade-off status indicated that some of the sampling plots were prone to “dried soil layer”. Among the vegetation parameters, R, H, Margalef, COHESION, and CONTAG showed reliable results in the fitting models for the trade-off status, while SPLIT showed regional not applicable. The three-dimensional surfaces were fitted by local regression to obtain zero trade-off inflection points (6 %–8%) and trend inflection points (7.5 %–9%) of soil moisture and VLI (effective) for typical sampling plots in the study area. Three-dimensional fitting model is more comprehensive and effective in assessing deep soil moisture conditions than two-dimensional models. Grass plots on shady slopes had the best trade-off status, while arbor-grass plots absorbed more water with the poorer ecological benefits.

The combination of sampling data and high-precision raster data offers a reference for investigating ecological benefits and vegetation restoration from point data to surface fitting in small watersheds. In this work, the parameter selection has limitations of regional characteristics because of the small study area. Further research should optimize the model mechanistically in a regional view and construct a large-scale model with compatible parameters. Additionally, combining field monitoring and image data will help explore regional ecological benefits for a long time and optimize a 3D model using deep soil moisture as a benchmark.

CRediT authorship contribution statement

Yuqing Chang: Conceptualization, Data curation, Investigation, Methodology, Validation, Writing – original draft, Writing – review & editing, Software. **Lei Han:** Conceptualization, Data curation, Funding acquisition, Investigation, Methodology, Resources, Software, Writing – original draft, Writing – review & editing. **Rui Chen:** Software. **Zhao Liu:** Investigation, Methodology, Resources. **Yabei Li:** Investigation. **Zilin Zhao:** Investigation. **Yifeng Gao:** Data curation, Investigation. **Meili Yang:** Data curation, Investigation. **Xinxin Cao:** Data curation. **Zheyuan Miao:** Data curation. **Hongliang Kang:** Data curation.

Funding

This study was funded by the National Natural Science Foundation of China (Program No. 41871190), the National Key Research and Development Program of China (No. 2023YFF1305105), the Fundamental Research Funds for the Central Universities, CHD (Program No. 300102353201), the Opening fund of the State Key Laboratory of Loess and Quaternary Geology, Institute of Earth Environment, CAS (Program No. SKLLQG2002). The sponsors had no role in the design, execution, interpretation, or writing of the study. We are grateful to the anonymous reviewers, whose comments have helped to clarify and improve the text.

Declaration of competing interest

The authors declare that they have no known competing financial interests or personal relationships that could have appeared to influence the work reported in this paper.

Data availability

The authors do not have permission to share data.

References

- Bradford, J.B., D'Amato, A.W., 2012. Recognizing trade-offs in multi-objective land management. *Front. Ecol. Environ.* 10 (4), 210–216. <https://doi.org/10.1890/110031>.
- Costa, L., Nunes, L., Ampatzidis, Y., 2020. A new visible band index (vNDVI) for estimating NDVI values on RGB images utilizing genetic algorithms. *Comput. Electron. Agric.* 172, 105334. <https://doi.org/10.1016/j.compag.2020.105334>.
- Fang, K., Song, N., Le, W., An, H., et al., 2012. Spatiotemporal distribution of soil moisture content and aboveground biomass under different terrains in desert steppe. *Arid Zone Res.* 29 (4), 641–647. <https://doi.org/10.13866/j.azr.2012.04.012>.
- Fischer, C., Leimer, S., Roscher, C., Ravenek, J., de Kroon, H., Kreutziger, Y., Baade, J., Beßler, H., Eisenhauer, N., Weigelt, A., et al., 2019. Plant species richness and functional groups have different effects on soil water content in a decade-long grassland experiment. *J. Ecol.* 107 (1), 127–141. <https://doi.org/10.1111/1365-2745.13046>.
- Frohn, R.C., 1997. *Remote Sensing for Landscape Ecology: New Metric Indicators for Monitoring, Modeling, and Assessment of Ecosystems*. CRC Press.
- Gao, X., Zhao, X., Wu, P., Brocca, L., Zhang, B., 2016. Effects of large gullies on catchment-scale soil moisture spatial behaviors: a case study on the Loess Plateau of China. *Geoderma* 261, 1–10. <https://doi.org/10.1016/j.geoderma.2015.07.001>.
- Gergel, S.E., Turner, M.G., 2017. *Learning Landscape Ecology: A Practical Guide to Concepts and Techniques*. Springer.
- Ghimire, C.P., Bruijnzeel, La., Lubczynski, M.W., Bonell, M., 2014. Negative trade-off between changes in vegetation water use and infiltration recovery after reforesting degraded pasture land in the Nepalese Lesser Himalaya. *Hydrol. Earth Syst. Sci.* 18 (12), 4933–4949. <https://doi.org/10.5194/hess-18-4933-2014>.
- Guo, Z., Wang, T., Liu, S., Kang, W., Chen, X., Feng, K., Zhang, X., Zhi, Y., 2021. Biomass and vegetation coverage survey in the Mu Us sandy land-based on unmanned aerial vehicle RGB images. *Int. J. Appl. Earth Obs. Geoinf.* 94, 102239. <https://doi.org/10.1016/j.jag.2020.102239>.
- Han, L., Chang, Y., Chen, R., Liu, Z., Zhao, Y., Zhu, H., Zhao, Z., Gao, Y., Yang, M., Li, Y., 2022. Response of soil moisture to vegetation and trade-off analysis in the hilly area of the Loess Plateau, China. *Ecol. Indic.* 142, 109273. <https://doi.org/10.1016/j.ecolind.2022.109273>.
- Jia, Y.-H., Shao, M.-A., 2014. Dynamics of deep soil moisture in response to vegetational restoration on the Loess Plateau of China. *J. Hydrol.* 519, 523–531. <https://doi.org/10.1016/j.jhydrol.2014.07.043>.
- Lamine, S., Petropoulos, G.P., Singh, S.K., Szabó, S., Bachari, N.E.I., Srivastava, P.K., Suman, S., 2018. Quantifying land use/land cover spatio-temporal landscape pattern dynamics from Hyperion using SVMs classifier and FRAGSTATS ®. *Geocarto Int.* 33 (8), 862–878. <https://doi.org/10.1080/10106049.2017.1307460>.
- Lin, X., Liu, Z., Chen, X., Lin, K., Cheng, L., 2021. Trade-off between carbon sequestration and water loss for vegetation greening in China. *Agric. Ecosyst. Environ.* 319, 107522. <https://doi.org/10.1016/j.agee.2021.107522>.
- Li, B., Gao, J., Wang, X., Ma, L., Cui, Q., Vest, M., 2016. Effects of biological soil crusts on water infiltration and evaporation Yanchi Ningxia, Maowusu Desert, China. *Int. J. Sediment. Res.* 31 (4), 311–323. <https://doi.org/10.1016/j.ijssrc.2016.05.005>.
- Li, Z., Tian, Y., Zhang, X., 2007. Study on the diversity of vegetation species in the Wuqi Chaogou watershed. *Soil Water Conserv. China* (4).
- Li, C., Yang, X., Liu, H., Zhu, H., Wei, H., Na, J., Cui, X., 2022. Spatial distribution characteristics of discontinuous hillslope gullies on the Loess Plateau of China: a special focus on spoon gullies. *Catena* 215, 106327. <https://doi.org/10.1016/j.catena.2022.106327>.
- Li, B., Zhang, W., Li, S., Wang, J., Liu, G., Xu, M., 2021. Severe depletion of available deep soil water induced by revegetation on the arid and semiarid Loess Plateau. *For. Ecol. Manage.* 491, 119156. <https://doi.org/10.1016/j.foreco.2021.119156>.
- Liang, W., Bai, C., Sun, B., Qi, J., 2006. Soil water effectiveness and water storage performance of fallow land in loess hilly areas: a case study of Chaogou watershed in Wuqi County, Shaanxi Province. *Bull. Soil Water Conserv.* 04, 38–40.
- Lifang, C., Qun, D., Zhiming, Z., Zehao, S., 2019. Moisture content variations in soil and plant of post-fire regenerating forests in central Yunnan Plateau, Southwest China. *J. Geogr. Sci.* 29 (7), 1179–1192. <https://doi.org/10.1007/s11442-019-1652-8>.
- Liu, L., Wang, Z., Wang, Y., Zhang, Y., Shen, J., Qin, D., Li, S., 2019. Trade-off analyses of multiple mountain ecosystem services along elevation, vegetation cover and precipitation gradients: a case study in the Taihang Mountains. *Ecol. Indic.* 103, 94–104. <https://doi.org/10.1016/j.ecolind.2019.03.034>.
- Ma, J., Wang, X., Zhao, X., Tian, L., Wang, Y., 2022. Experimental study of mulching effects on water restoration of deep, desiccated soil in a loess hilly region. *Environ. Technol.* 43 (22), 3462–3472. <https://doi.org/10.1080/09593330.2021.1922941>.
- Melliger, J.J., Niemann, J.D., 2010. Effects of gullies on space-time patterns of soil moisture in a semiarid grassland. *J. Hydrol.* 389 (3–4), 289–300. <https://doi.org/10.1016/j.jhydrol.2010.06.006>.
- Nan, G., Wang, N., Jiao, L., Zhu, Y., Sun, H., 2019. A new exploration for accurately quantifying the effect of afforestation on soil moisture: a case study of artificial Robinia pseudoacacia in the Loess Plateau (China). *For. Ecol. Manage.* 433, 459–466. <https://doi.org/10.1016/j.foreco.2018.10.029>.
- Shi, D., Tan, H., Rao, W., Liu, Z., Elenga, H.I., 2020. Variations in water content of soil in apricot orchards in the western hilly regions of the Chinese Loess Plateau. *Vadose Zone J.* 19 (1), e20034. <https://doi.org/10.1002/vzj2.20034>.
- Su, B., Su, Z., Shangguan, Z., 2021. Trade-off analyses of plant biomass and soil moisture relations on the Loess Plateau. *Catena* 197, 104946. <https://doi.org/10.1016/j.catena.2020.104946>.
- Tong, Y., Wang, Y., Song, Y., Sun, H., Xu, Y., 2020. Spatiotemporal variations in deep soil moisture and its response to land-use shifts in the Wind-Water Erosion Crisscross Region in the Critical Zone of the Loess Plateau (2011–2015), China. *Catena* 193, 104643. <https://doi.org/10.1016/j.catena.2020.104643>.
- Wang, S., Fu, B., Gao, G., Zhou, J., Jiao, L., Liu, J., 2015. Linking the soil moisture distribution pattern to dynamic processes along slope transects in the Loess Plateau, China. *Environ. Monit. Assess.* 187 (12), 1–13. <https://doi.org/10.1007/s10661-015-5000-x>.
- Wang, C., Wang, S., Fu, B., Li, Z., Wu, X., Tang, Q., 2017. Precipitation gradient determines the tradeoff between soil moisture and soil organic carbon, total nitrogen, and species richness in the Loess Plateau, China. *Sci. Total Environ.* 575, 1538–1545. <https://doi.org/10.1016/j.scitotenv.2016.10.047>.
- Wang, L., Wang, X., Chen, L., Song, N.P., Yang, X.G., 2020. Trade-off between soil moisture and species diversity in semi-arid steppes in the Loess Plateau of China. *Sci. Total Environ.* 750, 141646. <https://doi.org/10.1016/j.scitotenv.2020.141646>.
- Yan, G., Li, L., Coy, A., Mu, X., Chen, S., Xie, D., Zhang, W., Shen, Q., Zhou, H., 2019. Improving the estimation of fractional vegetation cover from UAV RGB imagery by colour unmixing. *ISPRS J. Photogramm. Remote Sens.* 158, 23–34. <https://doi.org/10.1016/j.isprsjprs.2019.09.017>.
- Yang, Y., Wang, B., Wang, G., Li, Z., 2019. Ecological regionalization and overview of the Loess Plateau. *Acta Ecol. Sin.* 39 (20), 7389–7397.
- Yun, K., Zhao, M., Mu, R., Guo, X., Ma, M., Wang, S., Zhang, X., Shang, H., 2014. Application of nonparametric quantile regression model in establishing medical reference intervals. *Chin. J. Health Stat.* 31 (3), 431–433.
- Zhang, Z., Ai, N., Liu, G., Liu, C., Qiang, F., 2021. Soil quality evaluation of various microtopography types at different restoration modes in the loess area of Northern Shaanxi. *Catena* 207, 105633. <https://doi.org/10.1016/j.catena.2021.105633>.
- Zhang, Q., Wei, W., Chen, L., Yang, L., 2018. Spatial variation of soil moisture and species diversity patterns along a precipitation gradient in the grasslands of the Loess Plateau. *J. Nat. Resour.* 33 (8), 1351–1362. <https://doi.org/10.31497/zrzyxb.20170726>.
- Zhang, X., Yang, G., Hu, J., Wang, D., 2008. Effect of different vegetation recovery modes on soil moisture ecoeffects in hilly and gully region of the Loess Plateau. *J. Nat. Resour.* 04, 635–642.